Reverse water-gas shift reaction at the Cu/ZnO interface: Influence of the Cu/Zn ratio on structure-activity correlations

Consuelo Álvarez Galván [b,1], Julia Schumann [a,1], Malte Behrens [c], José Luis García Fierro [b], Robert Schlögl [a,d], Elias Frei [a,*]

[a] Fritz-Haber-Institut der Max-Planck-Gesellschaft, Department of Inorganic Chemistry, Faradayweg 4-6, 14195 Berlin, Germany
[b] Instituto de Catálisis y Petroleoquímica (CSIC), C/Marie Curie, 2, Cantoblanco, 28049 Madrid, Spain
[c] Universität Duisburg-Essen, Fakultät für Chemie, Anorganische Chemie, CENIDE, Universitätsstr 7, 45141 Essen, Germany
[d] Department of Heterogeneous Reactions, Max-Planck-Institute for Chemical Energy Conversion, Stiftstrasse 34-36, 45470 Mülheim an der Ruhr, Germany

ARTICLE INFO

ABSTRACT

The physicochemical properties of hydroxycarbonate-based precipitates [zincian malachite (ZM) and aurichalcite precursors], calcined CuO/ZnO precatalysts and finally reduced Cu/ZnO catalysts, with several Cu-Zn ratios, have been investigated by different characterization techniques. Results from isothermal physisorption of N_2 (BET), X-ray Diffraction (XRD), Temperature Programmed Reduction (TPR), N_2O Reactive Frontal Chromatography (N_2O-RFC), X-ray Photoelectron Spectroscopy (XPS) and Scanning Electron Microscopy (SEM) have been correlated with the catalytic activity for the reverse water-gas shift (rWGS) reaction in order to provide insight into the controversial nature of active species in carbon dioxide activation, respectively the role of Cu and ZnO. Average crystalline domain size of CuO and ZnO show a relationship with the amount of each phase in the calcined sample. This is in agreement with the TPR profiles, which indicate a better dispersion of Cu for the ZnO-rich samples and a shift for the first reduction step to higher temperatures (T_{onset} for Cu^{II} to Cu^{I}). XPS measurements point out the surface enrichment of ZnO is less pronounced with higher ZnO/(ZnO + Cu) ratios. Activity results show that catalysts derived from high surface area ex-aurichalcite (Zn content, 50–70% atom) catalysts are more active in rWGS with lower apparent activation energies than ex-ZM catalysts (Zn content, 15–30% atom) with comparable apparent Cu surface area/N_2O capacity. Thus, the CO formation rate as function of the apparent Cu surface area indicates that the reaction rate is not dependent on the exposed apparent Cu surface, but from an adjusted interface composition predetermined by the precursor structure and its thermal post-treatment.

© 2016 Elsevier B.V. All rights reserved.

1. Introduction

Carbon dioxide has been attributed to be the main human source of the greenhouse effect. Nowadays, there are increasing attempts to consider it as a resource, rather than waste, since large amounts of low cost and relatively pure carbon dioxide will soon be available from carbon sequestration and storage facilities. The actual use of CO_2 is limited to a few processes like the syntheses of urea, salicylic acid and polycarbonates, but these only correspond to a small percentage of the potential CO_2 suitable for conversion to chemicals and/or fuels [1].

The catalytic conversion of CO_2 with H_2, via the reverse water-gas shift (rWGS) reaction, has been recognized as one of the most promising processes for CO_2 utilization. Synthesis gas could be used to produce hydrocarbons or oxygenated hydrocarbons via Fischer-Tropsch reaction, and also for the synthesis of methanol, a basic chemical for the production of synthetic fuels and polymers.

Among other formulations, Cu/ZnO based systems are active catalysts for the rWGS (Eq. (1)) [2], and for the synthesis of methanol (Eq. (2)) [3] at low temperatures (443–523 K).

$$CO_2 + H_2 \leftrightarrows CO + H_2O \qquad \Delta H_{298K} = 41\,kJ/mol \qquad (1)$$

$$CO_2 + 3H_2 \leftrightarrows CH_3OH + H_2O \qquad \Delta H_{298K} = -50\,kJ/mol \qquad (2)$$

Although methanol synthesis, as well as the (r)WGS reaction on Cu/ZnO have been investigated for several decades, many controversies still exist about the reaction mechanism and active sites of the catalyst.

A bare copper metal surface is widely regarded as the primary reaction center in the forward, the reverse shift and in methanol synthesis. Different and additional phases could have a role in the catalytic activity: Cu metal [4], Cu^+ in the lattice of ZnO [5,6], the Schottky barrier at the Cu-ZnO interface [7,8], defects in ZnO (oxygen vacancies) formed on the surface on ZnO crystals [9], active sites for CO and CO_2 chemisorption [6] or a strong metal-support interaction (SMSI effect) by which Cu particles are partially covered or encapsulated by ZnO [10,11] Additionally, promoters like alkali metals and rare earth metals as La etc. [12–14] influence the catalysts selectivity and activity. K_2O, for example, acts at the interface to Cu by weakening the bonding of surface intermediates [12].

Another important issue is the question, whether the rWGS reaction and methanol synthesis go through the same intermediate, or even happen at the same active site. According to Kunkes et al. [15], due to a different inverse kinetic isotope effect of H/D substitution, they do not share a common intermediate in the rate determining step.

It is generally accepted, that Zn plays an active role for methanol synthesis [16–18], but for the rWGS this is still controversial. Whereas some studies do not show a promotional effect of ZnO [16,17,19], others report that there is a beneficial effect of ZnO [20,21]. However, ZnO/Al_2O_3 catalysts are active in high temperature rWGS, where ZnO is seen as the active phase [22].

The role of CO_2 in methanol synthesis is ambiguous. On the one hand, it has been shown in isotope-labeled experiments under differential conditions, that CO_2 is the carbon source of methanol [18,23]. It is known as well, that CO_2 in the feed prevents the over-reduction of the ZnO component [24–26]. On the other hand, the formation of water as byproduct of the methanol synthesis from CO_2 and rWGS has an inhibitory effect on the activity, probably by blocking the active sites on the surface [27–29]. Further, CO can act as a scavenger for the surface water [30]. However, in order to get better control over the selectivity of the reaction pathway (methanol synthesis vs. rWGS reaction), it is necessary to understand both reactions and the role of the preparation history of the catalyst. This knowledge enables the design of catalysts with a high selectivity to methanol, as one key-compound in a non-fossil fuel based energy scenario.

Thus, the focus of this study is the influence of the nominal Cu/Zn ratio on the properties of the catalysts and its role in the reactivity in the rWGS reaction, decoupled from other influences like electronic and structural promoters.

Different binary Cu/ZnO catalysts have been prepared by a controlled and automatized co-precipitation method, which ensures the reproducibility of the catalyst synthesis. Furthermore, the influence of the precursor phases zincian malachite $[(Cu,Zn)_2(OH)_2CO_3)]$ and aurichalcite $[(Cu,Zn)_5(OH)_6(CO_3)_2]$ are analyzed on the microstructure and the resulting activity.

The different materials obtained during the genesis of the final catalyst samples, like copper and zinc hydroxycarbonates (precursors), calcined samples (precatalysts) and reduced samples (catalysts) have been thoroughly analyzed by different techniques (BET-SA, XRD, XRF, TPR, XPS and SEM). In the second part of the paper, the activities of the catalysts for the production of carbon monoxide and their activation energies by the rWGS reaction have been evaluated and correlated to their physicochemical properties. Because of the endothermic nature of the reaction, a high reaction temperature is favorable in the rWGS reaction to shift the equilibrium and generate more CO. However, we have used lower temperatures in the activity tests, since one goal of this study is to elucidate the reactivity of CO_2 and H_2 on Cu-ZnO catalysts for the comparison to the methanol synthesis reaction.

2. Experimental methods

2.1. Preparation of Cu-Zn catalysts precursors

As reported in the literature [31], the microstructural arrangement of CuO and ZnO particles in the catalyst precursor is determined by the physicochemical properties of the precipitates, that strongly depends on small variations in the precipitation and post-precipitation processes. Variations of the conditions such as the mode of adding the reactants, precipitation pH, ageing time, ageing temperature, washing, etc. are responsible for the so called "chemical memory" of the precipitates when they are converted into Cu/ZnO catalysts. According to previous studies, the Cu/Zn-precursors were prepared by a pH-controlled co-precipitation [32] in an automated reactor (LabMax from Mettler-Toledo). Different phases were systematically prepared: aurichalcite (Cu:Zn, 50:50, 40:60 and 30:70, molar ratios) and zincian malachite (Cu:Zn, 85:15, 80:20, 75:25 and 70:30). The proper amount of $Zn(NO_3)_2\cdot6H_2O$ and $Cu(NO_3)_2\cdot3H_2O$ was dissolved in Millipore water and 15 ml of concentrated HNO_3 to obtain 600 ml of a 1 M solution of the metal salts. This solution was added to the partially filled reactor at a constant rate of 20 ml/min. A Na_2CO_3 solution (1.6 M) was automatically added to keep the pH constant at 6.5. The precipitation temperature was adjusted to 338 K. The precipitation process was followed by an ageing time of 1 h (338 K, pH = 6.5), once the turbidity started to increase. The solid was then filter-collected and washed several times by redispersion in water until the conductivity of the washing medium was below 0.5 mS/cm. The solid hydroxy-carbonate precursors were obtained by spray drying. Calcination of the precursor for 3 h at 603 K yielded the CuO-ZnO precatalysts.

2.2. Characterization methods

XRD data were collected using a Bruker AXS D8 Advance Theta-theta diffractometer in Bragg-Brentano geometry, equipped with Cu anode, incident beam germanium monochromator (CuKα radiation) and scintillation counter. Measurements were taken between 4 and 80° 2θ with a step width of 0.5° and a counting time of 30 s/step. The diffractograms were analyzed by Rietveld fitting using the Topas software package [33] from Bruker AXS to extract the lattice parameters, estimate phase composition and determine the mean crystallite size from the L_{vol}-IB value.

BET surface area was calculated from isothermal N_2 adsorption (77 K) in a Quantachrome 6 port BET system. Prior to the measurements the samples were evacuated for 2 h at 373 K.

Temperature programmed reduction (TPR) studies have been conducted on a TPD/R/O 1100 instrument (CE Instruments). TPR studies were carried out by passing 5 vol.% H_2 (Ar) at a flow of 80 ml/min over a certain amount of the catalyst sample, maintaining the amount of copper oxide constant (25 mg). The temperature was increased to 573 K with a heating ramp of 6 K min^{-1}. The TPR data were deconvoluted with three Gauss functions using the software OriginPro9G®. The fit results are listed in Table 1 and in the SI (Fig. S3), exemplarily for CZ 85/15.

The apparent Cu^0 surface area (SA) of the reduced catalysts was measured by nitrous oxide (N_2O) chemisorption using the Reactive Frontal Chromatography (RFC) method [34]. Recent results revealed, that N_2O-RFC not only reacts with the Cu surface atoms, but also reacts with partially reduced ZnO_x species[35,36]. Therefore, the Cu-SA was overestimated in samples containing ZnO and we will refer to it as the apparent Cu^0-SA. Exposed Cu^0 and partially reduced ZnO_x surfaces of a pre-reduced Cu/ZnO catalyst were oxidized by switching the feed from an inert He stream to a reactive N_2O/He mixture. The N_2O capacity of the samples was calculated by quantifying the amount of released N_2. A detailed description of the experiment can be found in the SI.

Table 1
Chemical composition (XRF), d-spacing of the 20$\bar{1}$ reflection (XRD), BET surface area and selected reduction properties of the precatalysts.

Sample	Cu:Zn (XRF)	d(20-1) [Å]	BET [m^2/g]	T$_{onset}$ [K]	T$_{max}$ [K]	% area (1st peak)	% area (2nd + 3rd peak)
CZ 85-15	85:15	2.809	22	417	482	26	74
CZ 80-20	80:20	2.789	43	410	474	24	76
CZ 75-25	75:25	2.797	50	420	478	28	72
CZ 70-30	70:30	2.770	53	414	466	22	78
CZ 50-50	50:50	2.802	52	410	468	44	56
CZ 40-60	40:60	–	55	420	471	44	56
CZ 30-70	31:69	–	64	428	485	43	57

X-ray photoelectron spectra were recorded with a VG 200 R electron spectrometer operated in a constant pass mode and provided with a non-monochromatic MgKα ($h\nu$ = 1253.6 eV, 1 eV = 1.603 × 10^9 J) X-ray source operated at 10 mA and 12 kV. Prior to the analysis the reduced and passivated samples were subjected to reduction (493 K, in H$_2$ flow, for 10 min) in the treatment chamber of the spectrometer. The residual pressure in the ion-pumped analysis chamber was maintained below 4.2 × 10^{-9} mbar during data acquisition. The Cu 2p; Zn 2p; O 1s and C 1s energy regions were recorded for each sample and the respective binding energies (BE) were calibrated using the C 1s line at 284.9 eV as internal reference. BE values within an accuracy of 0.2 eV were obtained. Data processing was performed with the *XPS peak* program. For details see SI.

X-ray fluorescence spectroscopy (XRF) was performed of the precursor powder in a Bruker S4 Pioneer X-ray spectrometer. Scanning electron microscopy (SEM) images were taken in a Hitachi S-4800 field emission gun (FEG) system.

2.3. Activity tests

Preliminary runs were carried out to determine the proper catalyst particle size and reactant flow to avoid internal and external diffusion resistance, respectively.

Catalytic activity measurements were carried out in an 8-fold parallel reactor setup for rWGS. We used tubular quartz glass reactors with an inner diameter of 6 mm. The reactor was placed inside a programmable furnace and the temperatures were measured using type K thermocouples placed in the catalyst beds. 20 mg catalyst of a defined sieve fraction (0.1–0.2 mm) was diluted with SiC (140 mg), to improve heat transport and prevent hotspot formation. The bed height was 1 cm. Prior to the activity tests, the samples were reduced in situ in a 5% H$_2$ in N$_2$ flow (30 ml/min) with a heating ramp of 1 K min^{-1} to 523 K and a holding time of 30 min.

For the activity tests, a space velocity of 520 h^{-1} (GHSV) with respect to the H$_2$/CO$_2$ content was adjusted. The gas flows (H$_2$:CO$_2$:N$_2$ 1:1:8) were adjusted by mass flow controllers. The feed and product gas compositions were determined by online gas chromatography (GC), equipped with a thermal conductivity detector (TCD). Helium was used as the carrier gas and separation was accomplished using PPQ and mole sieve columns. The product gas composition was measured at 473 up to 503 K and reported values are averages from at least 3 consecutive analyses.

3. Results and discussion

3.1. Characterization of the precursors

The XRD patterns of the co-precipitated precursors show that for high Cu:Zn ratios (Cu content ≥ 70 at%), the zincian malachite (ZM) [(Cu,Zn)$_2$(CO$_3$)(OH)$_2$] phase dominates (Fig. 1).

The structure of the ZM phase can be derived from the malachite structure [Cu$_2$CO$_3$(OH)$_2$], by replacing some of the Cu^{2+} ions with Zn^{2+}. This replacement leads to changes in the lattice parameters,
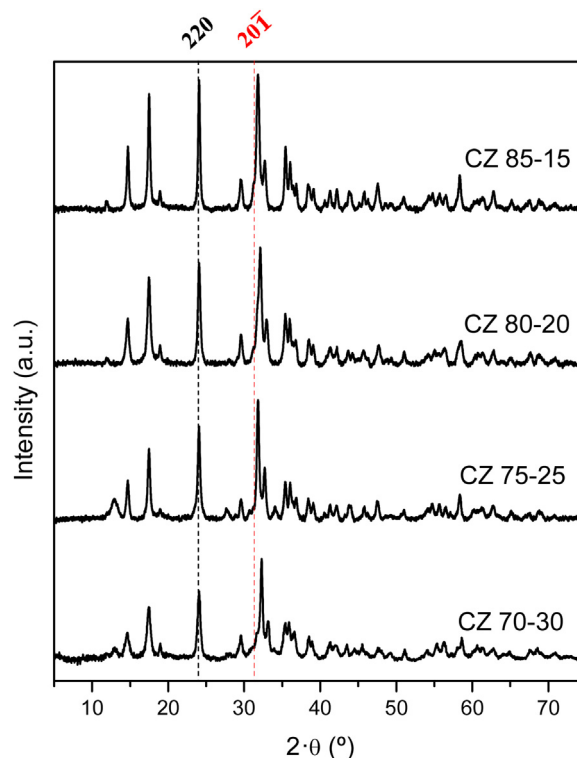

Fig. 1. XRD patterns of CuO/ZnO precursors (zincian malachite precursors).

e.g. contraction of the cell volume, as already noted by Porta et. al. [37] The most dominant change observed in the XRD pattern is the shift of the d(20$\bar{1}$) reflection (red line in Fig. 1 to guide the eye), which scales linearly with the amount of incorporated zinc [38,39]. This change is observed for our samples as well (Table 1).

For the precursors CZ 85-15 and CZ 80-20, pure ZM is obtained, while for CZ 75-25 and CZ 70-30, additionally a minor amount (<10%) of aurichalcite (AU) is present, seen at the additional reflex at 13° 2θ. This also explains the deviation of the d(20$\bar{1}$) value for CZ 75-25. Because of the enrichment of Zn in the AU byphase, a higher d(20$\bar{1}$) value (corresponding to a lower amount of Zn in the ZM structure) than expected is observed. For low Cu:Zn ratios (Cu contents ≤ 50 at%), the aurichalcite [(Cu,Zn)$_5$(CO$_3$)$_2$(OH)$_6$] is the main phase, with a minor zincian malachite impurity for the CZ 50-50 sample (see Fig. 2, red dotted box at 18° 2θ).

BET surface areas of the precursors decrease with increasing Cu content from 64 m^2/g for CZ 30-70 to 22 m^2/g for the copper richest CZ 85-15 sample (Table 1, Fig. 3). For the precursors with a similar elemental Cu:Zn ratio the BET-SA differences are less pronounced and in the range of 50 m^2/g. This is in accordance to the literature, which is in general very poor in precursor BET-SA values [40,41].

SEM micrographs show different morphologies for different precursor structures (Fig. 4). Thin platelets were found for the CZ 40-60 [AU, Fig. 4(b)] and rod-like particles for the CZ 80-20 (ZM,
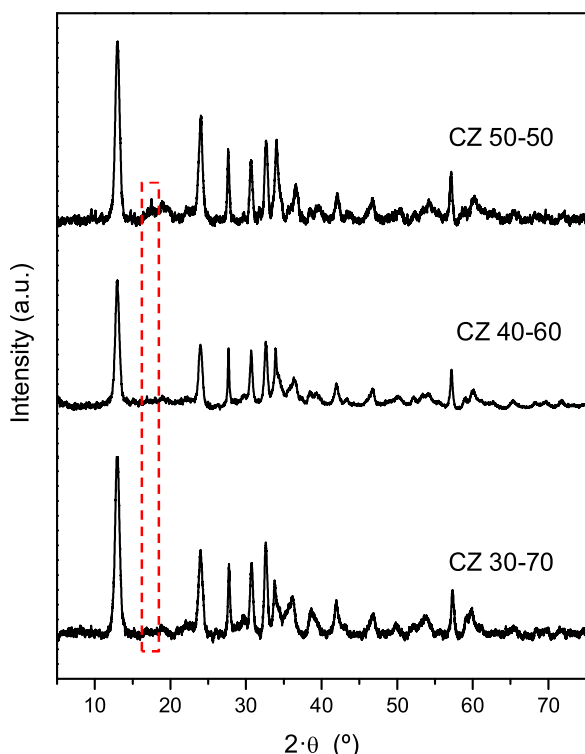
Fig. 2. XRD patterns of CuO/ZnO precursors (aurichalcite precursors).
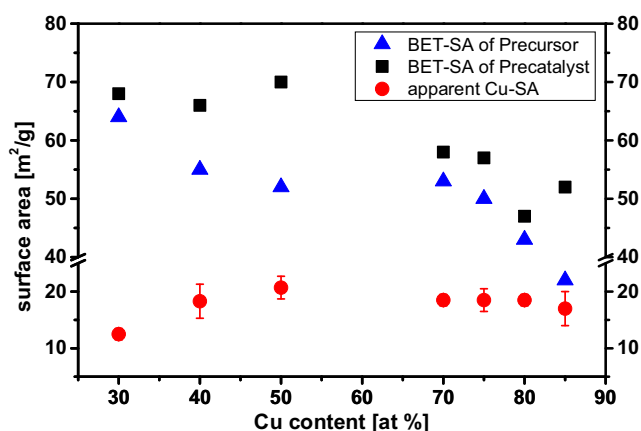

Fig. 3. BET surface areas vs Cu content for zincian malachite and aurichalcite precursors, precatalysts and apparent Cu-SA of catalysts.

Fig. 4(a) sample. The platelets of the AU precursors have a thickness in the range of 15 nm, whereas the thickness of the rods is in the range of 25 nm. The smaller microstructures found in the AU samples are in accordance with the higher surface areas obtained for these precursors.

XRF results show, that the Cu/Zn-ratios in the precursors correspond to their nominal values (see Table 1).

3.2. Characterization of the precatalysts

After the calcination, the precatalysts were characterized by: (i) X-ray Diffraction to determine the phase composition and crystallite size, (ii) by isothermal physisorption of N_2 at 77 K, to determine the surface area with the BET method and by (iii) temperature programmed reduction (TPR), to analyze the composition and interaction between different phases. All samples were completely reduced under the applied conditions, following the principles of Monti and Baiker [42]. A more detailed illustration of the TPR profiles and the normalized analysis is shown in the SI (Figs. S4 and S5).

After the calcination process, all the samples form particles of CuO and ZnO with crystalline domains smaller 7 nm (see Fig. 5). The results show a progressive growth of the crystallite size of the metal oxides with an increase of the corresponding cation ratio. That means for a high Cu-content small ZnO particles are obtained and for a high Zn-content small CuO-particles. Calcination of the precursors leads to an increase of the surface area for all samples (Figs. 3 and 5), in which the BET-SA decreases systematically with an increasing Cu-content. This trend agrees in principal with the precursors BET-SA values.

In accordance with some results reported in the literature for similar precursors, the surface area of the precatalysts reach a maximum value for the samples consisting of equal amounts of Cu and Zn [41]. However, higher Cu content leads to bigger, less dispersed particles with a lower surface area.

The reduction profiles of the precatalysts are displayed in Fig. 7 (left). Additionally, to monitor the reduction progress as a function of temperature and normalized time fractions, α-plots (integrated TPR curves, normalized) are shown (Fig. 7a–d). CuO gets step-wise reduced from Cu^{II} to Cu^{I} to Cu^{0} [42–44], this process is influenced by the reduction conditions (e.g. heating rate, here: constant for all samples) and sample properties (dispersion, particle size).

The Cu-rich samples fit very well with the XRD results of the precursors. The more Zn is incorporated into the ZM structure measures by the shift of the $d(20\bar{1})$ value, the less stable and earlier reducible is the resulting sample. This can be observed in the shift of the maximum temperature (T_{max}) of the reduction profiles of the calcined samples derived from ZM-precursors. Fig. 6 shows that the shift of the $d(20\bar{1})$ value correlates linearly with the T_{max} temperature of the TPRs, as evidence for a better dispersion and accessibility/reducibility of these Cu nanoparticles. The incorpo-
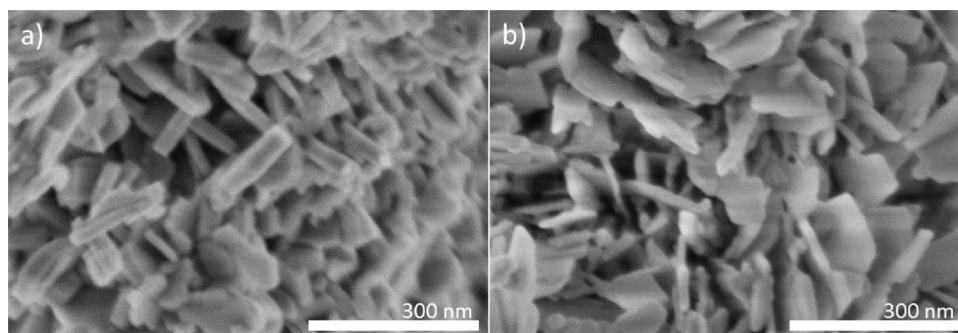

Fig. 4. SEM micrographs for zincian malachite (CZ 80-20) and aurichalcite (CZ 40-60) precursors.
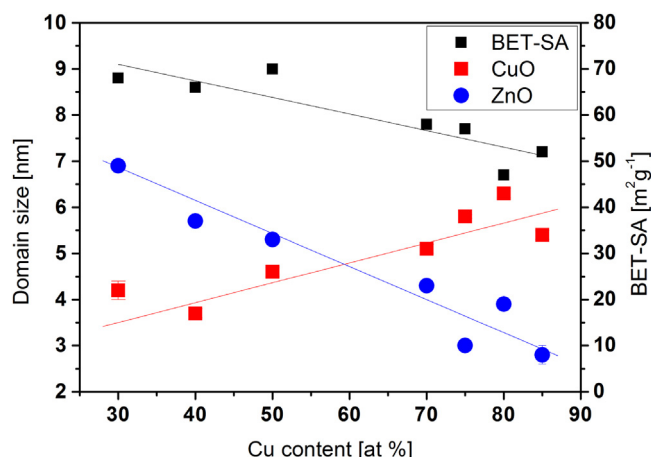
Fig. 5. Crystallite sizes of CuO and ZnO as a function of Cu content and the BET-SA.
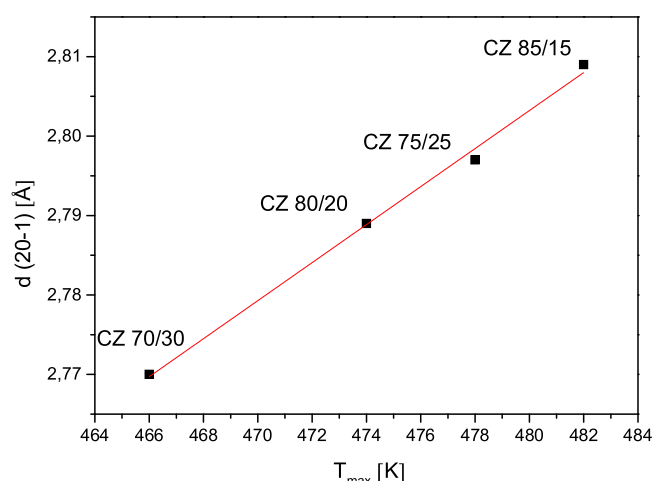

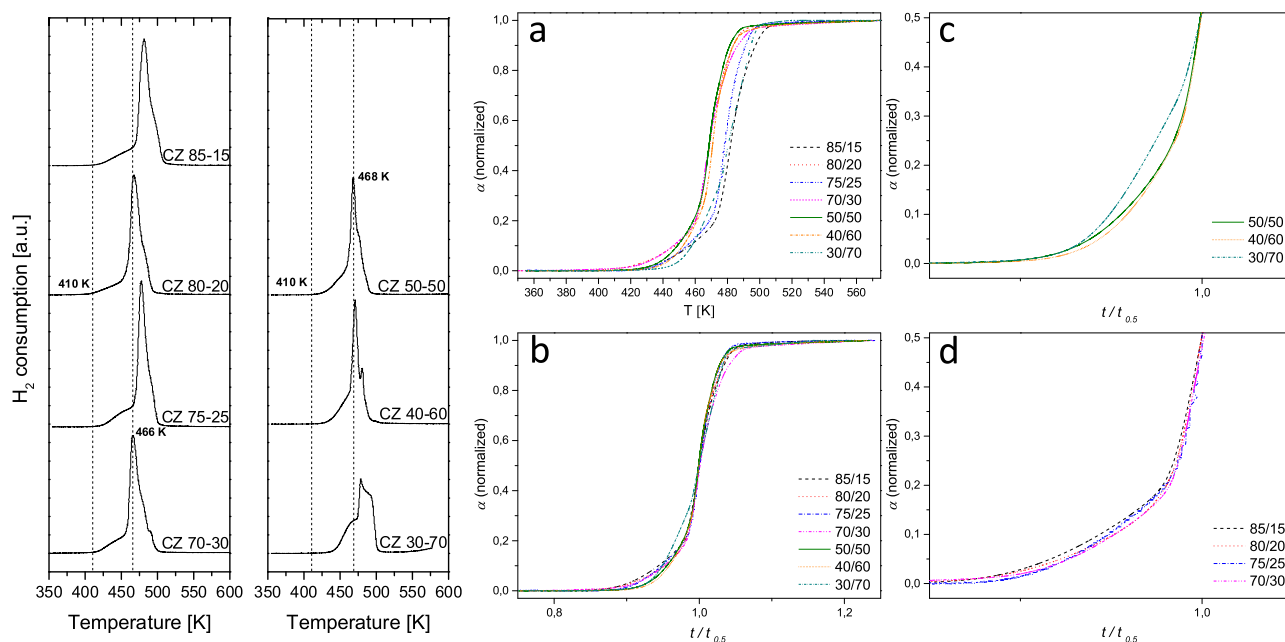**Fig. 6.** Correlation of the d(20-1) shift and the T_{max} in the TPR data.

ration of Zn in the malachite structure provides a homogeneous distribution of Zn on an atomic scale. The more Zn is incorporated the better is the CuO separation by ZnO in the precatalyst and the smaller stay the CuO particles (see domain sizes Fig. 5).

The Zn-rich samples show comparable T_{max} values to the CZ 70/30, excluding the CZ 30/70 sample which is shifted to higher reduction temperatures. The temperature shifts of the reduction profiles are visualized in Fig. 7a [α(normalized) vs.T]. A separation in early (CZ 80/20, CZ 70/30, CZ 50/50 and CZ 40/60) and late (CZ 85/15, CZ 75/25 and CZ 30/70) reducible precatalysts is shown.

Normalizing the integrated TPR curves to time-fractions (t/t$\alpha_{=0.5}$) provides additional valuable information about the reduction mechanism of the samples. The differences in Fig. 7b are in the range, where the general reduction behavior is identical. Separating the curves in Cu-rich (ZM-derived, Fig. 7d) and Zn-rich (AU-derived, Fig. 7c) samples show a slight variation until α = 0.5. The ZM-derived samples match perfectly with the results of the XRD-phase composition of the precursors. The temperature shifts in the TPR profiles describe well a particle size and dispersion effect of Cu steered by the degree of Zn^{2+} incorporation.

According to Table 1, the AU-derived samples show a larger area of the low-temperature shoulder, compared to the ZM-derived samples, which indicates that the Cu particles are more homogeneously distributed, better dispersed and equally accessible for the reduction process. This effect explains the properties of the precatalysts with respect to the trends in particle size (smaller), BET-SA (higher) and TPR (earlier).

3.3. Characterization of the catalysts

The activation treatment in a reductive atmosphere at 523 K, described in the experimental section, is sufficient to reduce the CuO crystallites in the precatalysts to Cu metal, evidenced by TPR. The reduced samples are characterized by N_2O decomposition to determine the apparent specific SA of Cu^0 and by XPS in order to analyze the surface composition.

Results obtained by the N_2O-RFC (Fig. 3 and Table S2 in SI), point out that the apparent Cu-SAs are close to 19 m^2/g for all the reduced samples, except for the sample CZ 30-70 (r), which presents a value around 12 m^2/g due to the small amount of Cu present in the sam-

Fig. 7. TPR profiles of the precatalysts.

Table 2
Surface atomic ratios of Cu/ZnO catalysts determined by X-ray Photoelectron Spectroscopy.

Catalyst	Nominal Zn/(Cu + Zn)	Surface Zn/(Cu + Zn)
CZ 85-15	0.15	0.54 (260%)[a]
CZ 80-20	0.20	0.61 (205%)[a]
CZ 75-25	0.25	0.72 (188%)[a]
CZ 70-30	0.30	0.70 (133%)[a]
CZ 50-50	0.50	0.82 (64%)[a]
CZ 40-60	0.60	0.80 (33%)[a]
CZ 30-70	0.70	0.83 (19%)[a]

[a] Comparison of the nominal and surface value of Zn/(Cu + Zn) ratio, to quantify the Zn-enrichment at the surface.

ple. The maximum value of 21 m^2/g is found for the catalyst CZ 50-50 with the same ratio of Cu and Zn and the highest BET-SA of the precatalysts. Although the amount of Cu is higher in the samples derived from ZM precursors, the apparent Cu-SAs are smaller. In these samples the proportion of ZnO seems not to be high enough to provide a better dispersion of the Cu phase, as also seen in the bigger domain size of CuO in the precatalysts. Additionally a more pronounced sintering during the reduction stage is likely [19]. As a consequence, the higher Cu loadings lead to bigger Cu particles and not to a bigger Cu-SA. The higher apparent Cu-SA of the CZ 50-50 sample, could also be originated in the similar particle sizes of ~5 nm for ZnO and CuO in the precatalyst, which avoids the sintering of Cu and facilitates a homogeneous distribution [35]. Furthermore, the contribution of the reduced ZnO species to the N$_2$O-RFC values needs to be considered. This seems to be higher for the samples with equal Cu and Zn content, leading additionally to a higher Cu/ZnO interface.

XPS measurements provide valuable information about the surface state and composition of the freshly reduced catalysts. As the binding energies of both Cu° and Cu$^+$ species are quite similar, the modified Auger parameters were calculated to differentiate which of these Cu species are present in the reduced catalysts. Typical values of this parameter around 1851.3 and 1849.5 eV were found in the literature for Cu° and Cu$^+$ species, respectively [45]. The binding energies of the core electrons and the modified Auger parameters (α_A) were determined for all the catalysts and obtained values are reported in Table S1. As representative spectra, the Cu 2p$_{3/2}$ photoelectron and Cu$_{LMM}$ Auger spectra of catalyst CZ 50-50 are shown in Fig. S1 (SI). As expected for lab source XPS measurements, the tiny differences in the spectra caused by a possible interface Cu$^{\delta+}$ is invisble and only Cu^0 is detected. Also, no significant variations in the binding energies for the Zn 2p$_{3/2}$ core level is measured, only ZnO and no direct spectroscopic evidence of a partially reduced ZnO$_x$ is observed (Table S1) [45–47].

The abundance of Zn as ZnO in the surface layer is derived for the integrated XPS data (Table 2). For all catalysts, an enrichment of Zn at the surface is occurring. This phenomenon is well known in the literature and commonly explained by the strong metal support interaction (SMSI) of Cu and ZnO [18,48–51].

Under reducing conditions ZnO$_x$ species partially cover the Cu surface [51,52]. The calculation of the relative surface Zn enrichment, comparing the surface Zn/Cu ratios and the nominal counterparts (values in brackets, Table 2 last column), evidences a trend of a lesser Zn surface enrichment with an increase of the nominal Zn/Cu ratio. This observation would also fit with the consecutive growth of the ZnO particle size in the precatalysts with the increasing Zn/Cu ratio (Fig. 5).

3.4. Activity tests of the catalysts

The activity for the rWGS reaction of the catalysts derived from the precursors with different Cu:Zn ratios was determined using
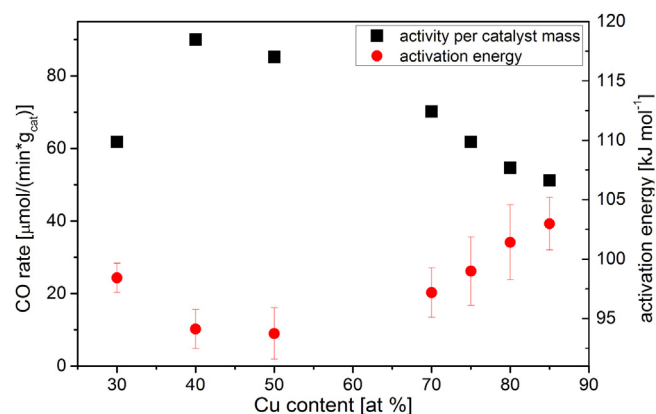

Fig. 8. CO formation rate per catalyst weight and activation energy as a function of Cu content for rWGS reaction at 503 K.

differential testing conditions, with CO$_2$ conversions below 4% in the entire temperature range (Fig. S2 in the SI) The activity per mass of the catalysts at 503 K and activation energies versus the Cu content are shown in Fig. 8.

These results indicate a better catalytic performance for the catalysts with similar proportions of Cu and Zn, derived from the aurichalcite enriched precursors. The most active catalyst is the CZ 40-60, closely followed by sample CZ 50-50 [19]. The lowest CO$_2$ conversion values for all the reaction temperatures are obtained for the CZ 85-15 catalyst, followed by the catalyst CZ 80-20 and CZ 75-25, all derived from a ZM phase (see also Fig. S2, SI). For the investigated samples higher activities correspond to lower apparent activation energies in rWGS reaction. The differences in the apparent activation energies are in the same range as reported in a study by Schumann et al. for Cu catalysts supported on differently doped ZnO (undoped 99 kJ/mol vs. doped 89 kJ/mol) [53]. Dopants like Ga^{3+} and Al^{3+} are structural and electronic promoters that influence e.g. the ZnO band-gap in the Cu/ZnO:M system and finally they facilitate the CO$_2$ activation (and dissociation) as rate determining step (RDS) of the rWGSR. The same effect is observable for the binary Cu/ZnO catalysts, the strongly ZnO enriched AU-derived catalysts show apparent activation energy differences of ~10 kJ/mol with respect to the Cu enriched samples [CZ 85/15 (103 kJ/mol) vs. CZ 40/60 (94 kJ/mol), see also Table S3]. Due to the fact that supported ZnO (ZnO/Al$_2$O$_3$) itself is an active high temperature rWGSR catalyst [22], it seems that the proper Cu/ZnO ratio provides an "activated ZnO" respectively an optimized Cu/ZnO interface for the CO$_2$ activation. The apparent activation energy and activity trends correlate only with the elemental ratios of Cu:Zn (similar ratios lower apparent activation energies, higher activities). No other trend is observable, neither the particles size of ZnO or Cu, nor any surface quantification. The XPS data give evidence that for an active interface the ZnO enrichment on the surface should be in the range of 70–80% (see Table 2). A ZnO enriched surface in the range of 60% (CZ 80/20 and CZ 85/15) shows a decrease in activity and increase in apparent activation energy in the rWGSR.

Referring to the reaction order of H$_2$ (0.11–0.15) and CO$_2$ (0.26–0.3) for H$_2$/CO$_2 \leq 3$ (Table S2, SI), the CO$_2$ activation is more critical. That means the rate determining step involves the CO$_2$ activation [54], and obviously the Zn-richer samples cope better with this, independent from their apparent Cu-SA [55]. This is shown with a plot of the activity data as a function of the apparent Cu-SA values (Fig. 9). For similar Cu-SA values (18–21 m^2/g), the ex-AU samples show a higher activity than the corresponding ex-ZM samples. This is a clear indication that the Cu/ZnO interface predetermined by the precursor structure is crucial, not the apparent Cu-SA. This finding is strongly supported by comparing the CZ
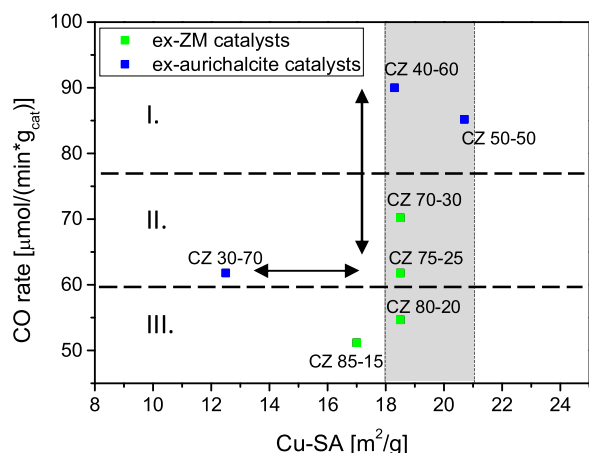
Fig. 9. CO formation rate as a function of Cu^0 surface area.

30/70, CZ 75/25 and CZ 40/60 catalysts in Fig. 9 (see black arrows): with completely different apparent Cu-SA the same activities in CO formation rate and almost identical apparent activation energies are observed for the CZ 30/70 and CZ 75/25 catalysts. A simple geometric argument (see Fig. S6) suggests these catalysts provide potentially the same quantity of Cu/ZnO interface (or ZnO/Cu; particle size difference ~3 nm). Consequently, the catalysts CZ 50/50 and CZ 40/60 with similar particles sizes (difference ~1–2 nm) and a potentially higher interface show a much higher activity. Due to the non-ideal spherical shape and the surface enrichment in ZnO a reliable quantification is not possible and thus the catalysts are separated into three groups according to their rWGS activity: I > II > III, steered by the elemental ratio and the potentially created interface.

This is in contrast to the results of Stone/Waller and others investigating binary Cu/ZnO catalysts for the rWGS reaction [17,19].

These findings support studies in which the rWGS reaction and the methanol synthesis do not share a common intermediate [15] and the CO_2 activation is not the RDS of the methanol synthesis, but a consecutive hydrogenation step at a Cu-enriched Cu/ZnO interface from zincian malachite derived catalysts [18,50]. The different character of the interface is part of a separated study and manuscript, investigated thoroughly by DRIFTS measurements.

4. Conclusions

A series of binary Cu/ZnO catalysts was prepared by calcination and reduction of either zincian malachite precursors (70 < Cu content < 85, atom%) or aurichalcite precursors (30 < Cu content < 50, atom%). SEM analyses show different morphologies for different precursor structures: thin sheets in case of aurichalcite and more massive, column-like rods for zincian malachite, which is in accordance with the lower BET surface areas of the precursors with increasing Cu content. The calcination of these precursors form a microstructure arrangement of CuO and ZnO particles with average crystallite domain sizes smaller 7 nm. The domain sizes of the oxides increase with an increase of the respective metal content. The reduction profiles suggest a higher, more homogeneous dispersion of CuO particles of precursors with similar elemental quantities, leading to an optimized CuO/ZnO contact, respectively a properly enriched ZnO surface quantified by XPS. Apparent copper surface areas of the Cu/ZnO catalysts are in the range of 19 m^2/g (except for CZ 30:70 sample). Activity results of these catalysts in the rWGS reaction show that ex-aurichalcite catalysts are more active than ex-zincian malachite catalysts independent from their apparent Cu-SA. This gives strong evidence that the interface between Cu and ZnO determines the catalytic activity. The character of the Cu/ZnO interface will be discussed in a separated

manuscript. The reaction order of H_2 (~0.1) and CO_2 (~0.3) shows that the activation of CO_2 is much more critical and that catalysts with an optimized ZnO enriched surface/interface perform much better. This is in accordance with the apparent activation energies, showing differences of ~10 kJ/mol for different catalysts. Following the interface argumentation, the quantity of the interface is given by the geometric perimeter dominated by the particles sizes of Cu and ZnO, the nature of the interface is adjusted by the Cu:ZnO ratio (see XPS data and apparent activation energies).

In summary, catalysts derived from the aurichalcite precursors with similar atomic proportions (Cu:Zn ratios 40:60 and 50:50) show homogeneously distributed CuO particles in ZnO, leading to higher activities and lower apparent activation energies in the rWGS reaction. This ZnO-enriched surface provides an optimized Cu/ZnO interface, for the activation and dissociation of CO_2 as RDS of the rWGS reaction.

Appendix A. Supplementary data

Supplementary data associated with this article can be found, in the online version, at http://dx.doi.org/10.1016/j.apcatb.2016.05.007.

References

[1] G. Centi, S. Perathoner, Catal. Today 148 (1–4) (2009) 191–205.
[2] Y. Tanaka, T. Utaka, R. Kikuchi, K. Sasaki, K. Eguchi, Appl. Catal. A 242 (2) (2003) 287–295.
[3] T. Ressler, B.L. Kniep, I. Kasatkin, R. Schlögl, Angew. Chem. 117 (30) (2005) 4782–4785.
[4] G.C. Chinchen, K.C. Waugh, D.A. Whan, Appl. Catal. 25 (1–2) (1986) 101–107.
[5] T.M. Yurieva, L.M. Plyasova, T.A. Kriger, V.I. Zaikovskii, O.V. Makarova, T.P. Minyukova, React. Kinet. Catal. Lett. 51 (2) (1993) 495–500.
[6] K. Klier, Methanol Synthesis, in: D.D. Eley, H. Pines, P.B. Weisz (Eds.), Adv. Catal., vol. 31, Academic Press, 1982, pp. 243–313.
[7] J.C. Frost, Nature 334 (6183) (1988) 577–580.
[8] F. Liao, Y. Huang, J. Ge, W. Zheng, K. Tedsree, P. Collier, X. Hong, S.C. Tsang, Angew. Chem. Int. Ed. 50 (9) (2011) 2162–2165.
[9] S. Miao, R.N. d'Alnoncourt, T. Reinecke, I. Kasatkin, M. Behrens, R. Schlögl, M. Muhler, Eur. J. Inorg. Chem. 2009 (7) (2009) 910–921.
[10] J.D. Grunwaldt, A.M. Molenbroek, N.Y. Topsøe, H. Topsøe, B.S. Clausen, J. Catal. 194 (2) (2000) 452–460.
[11] R. Naumann d'Alnoncourt, X. Xia, J. Strunk, E. Loffler, O. Hinrichsen, M. Muhler, Phys. Chem. Chem. Phys. 8 (13) (2006) 1525–1538.
[12] C.-S. Chen, W.-H. Cheng, S.-S. Lin, Appl. Cata. A: Gen. 238 (1) (2003) 55–67.
[13] R.T. Figueiredo, M.S. Santos, H.M.C. Andrade, J.L.G. Fierro, Catal. Today 172 (1) (2011) 166–170.
[14] K. Klier, C.W. Young, J.G. Nunan, Ind. Eng. Chem. Fundam. 25 (1) (1986) 36–42.
[15] E.L. Kunkes, F. Studt, F. Abild-Pedersen, R. Schlögl, M. Behrens, J. Catal. 328 (2015) 43–48.
[16] T. Fujitani, I. Nakamura, T. Uchijima, J. Nakamura, Surf. Sci. 383 (2–3) (1997) 285–298.
[17] I. Nakamura, T. Fujitani, T. Uchijima, J. Nakamura, Surf. Sci. 400 (1) (1998) 387–400.
[18] M. Behrens, F. Studt, I. Kasatkin, S. Kuhl, M. Hävecker, F. Abild-Pedersen, S. Zander, F. Girgsdies, P. Kurr, B.L. Kniep, M. Tovar, R.W. Fischer, J.K. Norskov, R. Schlögl, Science 336 (6083) (2012) 893–897.
[19] F.S. Stone, D. Waller, Top. Catal. 22 (3) (2003) 305–318.
[20] J.A. Rodriguez, P. Liu, J. Hrbek, J. Evans, M. Pérez, Angew. Chem. Int. Ed. 46 (8) (2007) 1329–1332.
[21] Y. Yang, J. Evans, J.A. Rodriguez, M.G. White, P. Liu, Phys. Chem. Chem. Phys. 12 (33) (2010) 9909–9917.

[22] S.-W. Park, O.-S. Joo, K.-D. Jung, H. Kim, S.-H. Han, Appl. Catal. A: Gen. 211 (1) (2001) 81–90.
[23] G.C. Chinchen, P.J. Denny, D.G. Parker, M.S. Spencer, D.A. Whan, Appl. Catal. 30 (2) (1987) 333–338.
[24] B. Denise, R.P.A. Sneeden, B. Beguin, O. Cherifi, Appl. Catal. 30 (2) (1987) 353–363.
[25] D.S. King, R.M. Nix, J. Catal. 160 (1) (1996) 76–83.
[26] J.S. Lee, K.H. Lee, S.Y. Lee, Y.G. Kim, J. Catal. 144 (2) (1993) 414–424.
[27] K. Fujimoto, Y. Yu, Second Int. Conf. Spillover (1993) 393.
[28] T. Inui, T. Takeguchi, Catal. Today 10 (1991) 95.
[29] E. Kunkes, M. Behrens, Chemical Energy Storage, in: R. Schlögl (Ed.), De Gryter, Berlin/Boston, 2013, pp. 4422–4426.
[30] C. Yang, Z. Ma, N. Zhao, W. Wei, T. Hu, Y. Sun, Catal. Today 115 (1–4) (2006) 222–227.
[31] B. Bems, M. Schur, A. Dassenoy, H. Junkes, D. Herein, R. Schlögl, Chem. Eur. J. 9 (9) (2003) 2039–2052.
[32] M. Behrens, J. Catal. 267 (1) (2009) 24–29.
[33] A.A. Coelho, TOPAS General Profile and Structure Analysis Software for Powder Diffraction Data, Bruker AXS GmbH, Karlsruhe, Germany, 2006 (version 3.0).
[34] G.C. Chinchen, C.M. Hay, H.D. Vandervell, K.C. Waugh, J. Catal. 103 (1) (1987) 79–86.
[35] M.B. Fichtl, J. Schumann, I. Kasatkin, N. Jacobsen, M. Behrens, R. Schlögl, M. Muhler, O. Hinrichsen, Angew. Chem. Int. Ed. 53 (27) (2014) 7043–7047.
[36] S. Kuld, C. Conradsen, P.G. Moses, I. Chorkendorff, J. Sehested, Angew. Chem. Int. Ed. 53 (23) (2014) 5941–5945.
[37] P. Porta, S. De Rossi, G. Ferraris, G. Minelli, G. Moretti, J. Catal. 109 (2) (1988) 367–377.
[38] M. Behrens, F. Girgsdies, Z. Anorg. Allg. Chem. 636 (6) (2010) 919–927.
[39] S. Zander, B. Seidlhofer, M. Behrens, Dalton Trans. 41 (2012) 13413–13422.
[40] Y. Okamoto, K. Fukino, T. Imanaka, S. Teranishi, J. Phys. Chem. 87 (19) (1983) 3740–3747.
[41] J. Agrell, M. Boutonnet, I. Melián-Cabrera, J.L.G. Fierro, Appl. Catal. A 253 (1) (2003) 201–211.
[42] D.A.M. Monti, A. Baiker, J. Catal. 83 (2) (1983) 323–335.
[43] A. Tarasov, S. Kühl, J. Schumann, M. Behrens, High Temp. High Press 42 (2013) 377–386.
[44] S. Kühl, A. Tarasov, S. Zander, I. Kasatkin, M. Behrens, Chem. Eur. J. 20 (13) (2014) 3782–3792.
[45] C.D. Wagner, L.H. Gale, R.H. Raymond, Anal. Chem. 51 (4) (1979) 466–482.
[46] L. Alejo, R. Lago, M.A. Peña, J.L.G. Fierro, Appl. Catal. A 162 (1–3) (1997) 281–297.
[47] B. Peplinski, W.E.S. Unger, I. Grohmann, Appl. Surf. Sci. 62 (3) (1992) 115–129.
[48] W.P.A. Jansen, J. Beckers, J.C. v. d. Heuvel, A.W. Denier v. d. Gon, A. Bliek, H.H. Brongersma, J. Catal. 210 (1) (2002) 229–236.
[49] J. Sloczynski, R. Grabowski, P. Olszewski, A. Kozlowska, J. Stoch, M. Lachowska, J. Skrzypek, Appl. Catal. A 310 (2006) 127–137.
[50] J. Schumann, T. Lunkenbein, A. Tarasov, N. Thomas, R. Schlögl, M. Behrens, ChemCatChem 6 (10) (2014) 2889–2897.
[51] T. Lunkenbein, J. Schumann, M. Behrens, R. Schlögl, M.G. Willinger, Angew. Chem. Int. Ed. 54 (15) (2015) 4544–4548.
[52] M.G. Sanchez, J.L. Gazquez, J. Catal. 104 (1) (1987) 120–135.
[53] J. Schumann, M. Eichelbaum, T. Lunkenbein, N. Thomas, M.C. ÁlvarezGalván, R. Schlögl, M. Behrens, ACS Catal. 5 (6) (2015) 3260–3270.
[54] S.-I. Fujita, N. Usui, N. Takezawa, J. Catal. 134 (1) (1992) 220–225.
[55] M.J.L. Ginés, A.J. Marchi, C.R. Apesteguía, Appl. Catal. A 154 (1–2) (1997) 155–171.